

Article

A Method for Large Underground Structures Geometry Evaluation Based on Multivariate Parameterization and Multidimensional Analysis of Point Cloud Data

Adam Wróblewski , Jacek Wodecki , Paweł Trybała  and Radosław Zimroz * 

Department of Mining, Faculty of Geoengineering, Mining and Geology, Wrocław University of Science and Technology, 50-370 Wrocław, Poland

* Correspondence: radoslaw.zimroz@pwr.edu.pl

Abstract: In underground mining, new workings (tunnels) are constructed by blasting or mechanical excavation. The blasting technique used in underground mines is supported by economic aspects, especially for deposits characterized by hard rocks. Unfortunately, the quality of the result may be different than expected in terms of the general geometry of work or the roughness of excavation surfaces. The blasting technique is also a source of vibrations that may affect other existing structures, affecting their stability. Therefore, it is of great importance to monitor both the quality of the new tunnels and changes in existing tunnels that may cause rockfall from the sidewalls and ceilings of both new and existing tunnels. The length of mining tunnels and support structures in underground mines is massive. Even if one would like to limit monitoring of tunnel geometry to those used every day for major technological processes such as transport, it is a vast amount of work. What is more, any stationary monitoring system is hard to utilize both due to everyday blasting procedures and mobile machine operation. The method proposed here is based on quick LiDAR/Terrestrial Laser Scanner measurements to obtain a cloud of points, which allows generating the spatial model of a mine's geometry. Data processing procedures are proposed to extract several parameters describing the geometry of the tunnels. Firstly, the model is re-sampled to obtain its uniform structure. Next, a segmentation technique is applied to separate the cross sections with a specific resolution. Statistical parameters are selected to describe each cross section for final 1D feature analysis along the tunnel length. Such a set of parameters may serve as a basis for blasting evaluation, as well as long-term deformation monitoring. The methodology was tested and validated for the data obtained in a former gold and arsenic mine Złoty Stok, Poland.

Keywords: underground mining; mining excavations; tunneling; LiDAR; terrestrial laser scanning; point cloud; 3D model; statistical features; geometry measurement and analysis; dimensionality reduction; principal component analysis



Citation: Wróblewski, A.; Wodecki, J.; Trybała, P.; Zimroz, R. A Method for Large Underground Structures Geometry Evaluation Based on Multivariate Parameterization and Multidimensional Analysis of Point Cloud Data. *Energies* **2022**, *15*, 6302. <https://doi.org/10.3390/en15176302>

Academic Editor: Krzysztof Skrzypkowski

Received: 29 July 2022

Accepted: 25 August 2022

Published: 29 August 2022

Publisher's Note: MDPI stays neutral with regard to jurisdictional claims in published maps and institutional affiliations.



Copyright: © 2022 by the authors. Licensee MDPI, Basel, Switzerland. This article is an open access article distributed under the terms and conditions of the Creative Commons Attribution (CC BY) license (<https://creativecommons.org/licenses/by/4.0/>).

1. Introduction

In many underground mines worldwide, especially those operating in hard rocks, the drilling and blasting technique is the most commonly used method to excavate valuable material [1]. This technique is relatively cheap and provides high flexibility of operations. Although drilling and blasting technology has been strongly optimized over the years [2], there are still some major issues to overcome. One of them is the appropriate design of this process to prevent over- and underbreaks [3] together with the prediction of high risk of potential over- and under-excavated zones [4]. From the geometry point of view, it is not so easy to control and maintain the actual shape of the tunnel cross section defined in the blast plan in the presence of hard geological conditions, manifested in the inhomogeneity of the rock mass.

Geological and mining conditions are the main determinants of the design of the excavations [5]. The over- and underbreaks that occur after the drilling and blasting procedure are a serious problem, as they are not in line with the defined parameters selected under these conditions. The deviations from the assumed cross section in the form of underbreaks make the excavations insufficient for the proper operation of mining machines and devices required for the materials extraction processes. Moreover, limited dimensions of mine tunnels endanger the underground crew, determined by the permissible concentration of oxygen and harmful gases in the mine air, its temperature, and the intensity of its flow [6]. Underbreaks resulting from inaccurate drilling and blasting need to be removed by additional drilling and blasting, increasing excavation maintenance costs. On the other hand, overbreaks also contribute to increasing operating costs. As the part of the rock mass not intended for excavation, overbreak material is often non-usable and when blasted, degrades the ore, generating additional costs at the processing level. Enlarged dimensions of the excavations may also lead to issues with stability [7]. For these reasons, there is a strong need for sufficient control and prevention of over- and underbreaks.

Although there have been numerous approaches tested and validated that help avoid over- and underbreaks, there are still some hard to control factors, e.g., the complexity of the rock mass or human factors that result in an increase or decrease in the size of tunnels compared to the design. In some cases, the already adopted drill-and-blast technique may not be the most efficient, especially in rapidly changing geological and mining conditions. There is a strong need not only for over- and underbreak prevention but also for a quick and reliable method to measure and assess the quality of underground excavations for further decision making.

Moreover, since drilling and blasting is often outsourced, there is a need to develop a method for quick evaluation of mining tunnel geometry, in other words, work quality assessment. This is a particularly important matter when additional expenditures must be incurred for extra drilling and blasting due to underbreaks, as well as concreting or other techniques to overcome overbreaks. Furthermore, each sequence of blasting may negatively influence the stability of the tunnel directly or induce seismic shocks. Especially in deep mines, it is clear that there is additionally a convergence of mine tunnels that should be monitored on a regular basis.

As shown above, measurements of geometry are an important topic in underground mining. Shapes of tunnels, pillars, and excavations change over time, influencing the stress distribution in a rock mass [8]. This leads to the deformation of the tunnels. They must be monitored to ensure the acceptable speed of deformation development, thereby enabling safe and continuous operation of the mine. Another issue requiring geometric measurements is the excavation process. Metric methods of tracking the mining progress allow us to not only estimate the volume of extracted material [9] but also to check the actual excavation geometry compliance with the overall plan. This is especially important in the case of employing mining techniques such as drilling and blasting, which often cause unpredicted changes of the blasting site geometry and put additional stress on the rock mass. An ideal solution for those problems is frequent monitoring with modern methods for a 3D metric reconstruction of the underground sites, such as photogrammetry or laser scanning [10–12]. However, since the quality of the former is vastly influenced by the lighting conditions, the latter method is usually the preferred one in harsh deep mining environments. Laser scanning produces data in the form of an unstructured point cloud: an abundant set of points with coordinates in 3D space, usually characterized by additional variables, such as the intensity of the laser beam reflection. The problem of analyzing such data is often the enormous size of the point cloud and the lack of topological information of spatial relationships between points [13,14]. To get from the raw measurement data to a tunnel convergence estimation or a blasting quality assessment accessible for interested parties such as the geomechanical engineers or stakeholders, an automated and scalable procedure is needed. Such a procedure should allow approximation of the structure from a point cloud, analyzing its irregularities and deviations from the plan or prediction, and

presenting them in an action-enabling way, conceivably with a model characterized by easily understandable parameterized metrics.

In this paper, we propose a methodology for geometry analysis based on a 3D scanning procedure and spatial data processing. In general, the idea of 3D scanning is well known in tunneling, but the key issue is related to 3D data modeling and analysis with the focus on features extraction, their analysis, and interpretation. It makes the mining workings case different from a tunnel inspection case.

The paper is organized as follows: firstly, the most important approaches used in tunnel inspection are recalled. Secondly, mining workings being analyzed and experimental works performed (scanning devices, procedure, and experiment) are described. The novelty of the paper is related to the methodology developed for 3D data analysis. Thus, the results of 3D data analysis are presented for experiments performed in the underground mine in the final part of this article.

2. State of the Art

Blasting is commonly used to mine hard rocks. This is a critical process from several perspectives. It is obvious that one should mention safety issues, financial aspects, quality of rock fragmentation, tunnel geometry that results from blasting, etc. In this paper, we focus on “quality of blasting” related to the planned mapping of the geometry of the tunnel into the real shape of the tunnel after blasting. Appropriate geometry of the tunnel is important for many other processes (tunnel maintenance, ventilation, transport, etc.). As the usual underground mine includes several hundred kilometers of tunnels, there is a need to provide a procedure to monitor mining workings in a long-term sense as well as to assess the compatibility of planned and received geometry just after blasting.

The over- and underbreaks can be brought about by two main reasons: by the drill-and-blast design and execution and by the geomechanical features of the rock mass [15]. Thus, many scientists in their research have raised the problem of drilling and blasting parameter selection to ensure the predefined shape of excavation [16–18].

The second main cause of over- and underbreaks together with the drill-and-blast factors have been studied more carefully. The role of geological discontinuities in causing blasting over- and underbreaks of the minor (<3 m) and major (>3 m) scale has been evaluated by [19] through joint analysis. In [20], multiple regression analysis, both linear and non-linear (LMRA and NMRA), and artificial neural network (ANN) were applied to forecast overbreaks and assess the influence of geological parameters based on 49 sets of overbreak and rock mass rating (RMR) data. In [21], the authors used data from 18 blasting experiments conducted on-site during construction of a highway tunnel in China as a feed for machine learning. To map the dependencies between the geological conditions, control indices, and the outputs of the smooth blasting parameters, the improved support vector regression (ISVR) model was implemented. In addition, an ISVR algorithm was supported by a genetic algorithm (GA) to automate the choice of optimal parameters of the ISVR model. Similarly, linear multiple regression analysis was performed in [22] to predict the overbreaks induced by blasting. Controllable, non-controllable (geological conditions), and semi-controllable blast factors were studied. Operative methodology to differentiate drill-and-blast-related overbreaks from geological ones, together with its volume estimation procedure, was presented in [23].

To estimate the size of under- and overbreaks, an appropriate measurement method that provides data high quality and easy collection is required. Maerz et al. [24] divided the excavation profile’s measurement techniques into surveying ones (manual or laser) and photographic light sectioning methods. Simply stated, manual methods consist of determining the distance between the certain central point to the tunnel boundaries at fixed angular intervals. Utilized in the past, manual methods are time-consuming and strongly inefficient when the high accuracy of measurements is needed on long tunnels.

A promising method has been proposed in [25]. Cross-section measurements through a light sectioning method are performed by outlining it with a plane of light from a conical

mirror. Although the procedure is much faster than the manual ones, there is still a need to manually process the photographs and estimate the size of over- and underbreaks. Nowadays, laser techniques are being exploited, ensuring high accuracy and enabling automatic post-processing.

LiDAR, defined as *Laser Induced Detection and Ranging* or *Light Detection and Ranging*, is a laser-based device allowing users to measure the distance between the sensor and other objects [26]. It is obtained thanks to its active sensor high frequency spins emitting a laser beam, which is reflected from the object and received back, allowing precise determination of the position of the object in relation to the sensor. LiDAR can operate in two different modes: sending short pulses or continuous signals. Based on this, the distance is obtained through Time-of-Flight (ToF) of the laser beam or phase-shift estimation of the electromagnetic wave that returns to the sensor relative to the output electromagnetic wave. Generally, the better sensing range is exhibited by ToF Terrestrial Laser Scanners, while phase-based devices give higher accuracy. As a result of laser scanner measurements, a precise and dense point cloud is obtained, which is the set of coordinates of points in a three-dimensional coordinate system. Numerous reflections of the same, scattered beam of different strength may be detected by the LiDAR and used for sophisticated data analysis, together with other features provided, e.g., intensity or reflectance of the beam [27].

Laser scanning is used in the urban tunnel's geometry reconstruction in the form of a 3D point cloud. Deformation estimation based on terrestrial laser scanning as a part of tunnel structural monitoring is presented in [28]. The 3D laser scanning for structural inspection of the tunnels performed under an autonomous UGV mission for concrete lining tunnel inspection is shown in [29]. Amedjoe and Agyeman [30] presented a mine excavations stability problems management approach based on cavity monitoring system data captured in the AngloGold Ashanti–Obuasi Mine. In order to reduce the number of accidents related to rock falls, Warneke et al. [31] applied 3D laser scanning technology to assess tunnels' geometry drifts and overbreaks in Stillwater Mine, Montana. Zou et al. [32] presented a smooth blasting evaluation method thanks to a mobile app utilizing geometry-related data captured by a laser profilometer.

Moreover, in recent years, 3D laser scanning techniques have been applied widely in other tunneling and mining applications [33,34]. As convergence monitoring is a well-known tunneling problem [35–40], the authors in [40] proved that data provided by a mobile LiDAR system can be used as an input for the method that automatically detects road tunnel luminaries.

The scanning technology is also very useful for specific mining applications. For example, Vanneschi et al. [41] successfully applied 3D scanning data for rock pillar degradation monitoring, while Xu et al. [42] proposed to use terrestrial laser scanning for water leakage. In [43], it is advised to use laser scanning technology on incident investigations in the mining industry. The authors in [44] considered the usage of scanning for drill and blast excavation forecasting. A review of commercial mobile mapping and surveying solutions suitable for GNSS-denied environments, such as underground mines, has been provided in [45].

Carrying out the LiDAR field measurements does not yet result in an easy to interpret model, as the data should be preprocessed using automated procedures to avoid mundane manual model preparation. The appropriate method for subsequent data analysis is also very important. In [46], the authors proposed a method for continuous extraction of subway tunnel cross sections based on terrestrial point clouds. In [47], the authors developed an automated and efficient method for extraction of tunnel cross sections using terrestrial laser scanned data. Raw 3D data from scanning are not suitable for tunnel condition evaluation, thus in [48] a procedure for feature extraction of a concrete tunnel liner from 3D laser scanning data has been proposed.

The next step is to provide a data-driven decision support system. The major issues in designing such a system, also applicable in this study, are the identification or creation of a crucial variable for decision making and providing thresholds or more sophisticated

methods to interpret its values. Often, machine learning techniques are used for those purposes. A Back Propagation Neural Network (BPNN) and Multivariate Adaptive Regression Splin (MARS) machine learning algorithm has been proposed in [49,50]. It was already mentioned above that multiple regression analysis and artificial neural network (ANN) were applied to forecast the overbreaks in [20]. In [33], a state-of-the-art review focusing on segmentation and classification of mobile laser scanning point clouds is presented. For more details, one may refer to review papers by Grilli [51] or Remondino et al. [52,53].

3. Experiments and Data Description

3.1. Złoty Stok Gold Mine

Złoty Stok is a town located in Lower Silesia Province, southwestern Poland, in the Eastern Sudetes. The city owes its name to the former gold exploitation from the 13th century. At a later stage of the mine's operation, arsenic ore was mined there until 1961.

The geological structure of the rock mass in which the tunnels are located is quite complex. The presence of the Złoty Stok—Skrzzynka tectonic zone, which is a part of the Ladek—Śnieżnik metamorphic structure, is the reason for phenomena of cataclasis and mylonitization of varying intensity in the Złoty Stok area. Metamorphic rocks are represented by schists (mica, mica–quartz, and quartzite schists), but also gneisses, leptynites, amphibolites, as well as serpentinites and crystalline limestones gneisses are common. Rocks in the Złoty Stok–Skrzzynka tectonic zone and Kłodzko–Złoty Stok Massif borders are contact-altered and cut by faults and dislocation zones [54].

From a huge complex of excavations (see Figure 1) consisting of over 300 km of underground corridors, located on 21 levels, only 2 adits are accessible since in 1996 an underground tourist route named “Kopalnia Złota” (Gold Mine) was opened. The first one, Gertruda adit, is two kilometers long, but only initial 500 m can be seen. The remaining part of this slant is deprived of lighting and flooded with water, and merely a small part can be visited with boats. The second one, Czarana adit, is also partially opened. One of its side corridors (approx. 200 m long) leads to a 25 m shaft from the 17th century, giving access to a huge chamber in which a unique, 8-meter long underground waterfall can be seen.

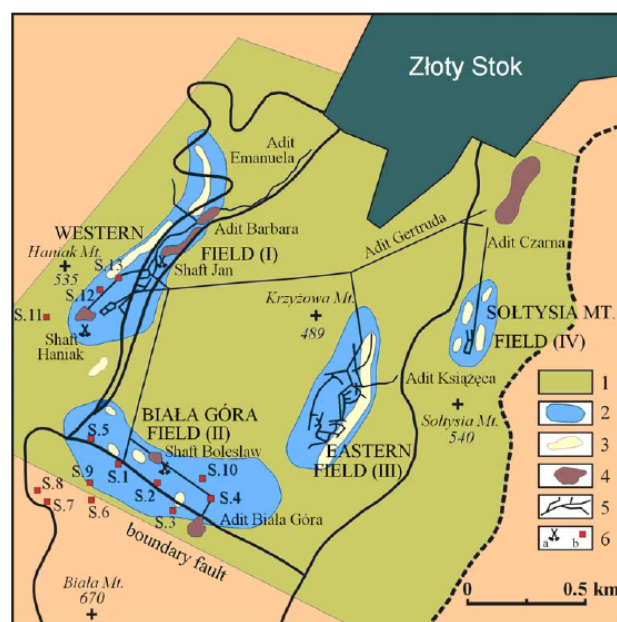


Figure 1. Złoty Stok post mining area [55]. Legend: 1—mining area; 2—limestones; 3—ore nests; 4—mining waste heaps; 5—slants, galleries, and adits; 6—shafts.

The deep and extensive mine excavations in the Złoty Stok Mine were made entirely by hand, then by blasting in very hard, though fractured massif of metamorphic rocks. Thus, this mine has been selected for testing purposes, firstly, because it is an old mine

in which the problem with corridor geometry (roughness/unevenness of surface) is very clearly visible. Secondly, because it is more available than deep underground mines in operation. The unique characteristic of the workings is the reason for some other interesting papers related to experimental works in this mine [56,57].

3.2. Data Collection

For the purpose of testing the methodology developed in this study, data from the work concerning the accuracy evaluation of a LiDAR SLAM solution, namely High-Density LiDAR SLAM (HDL-SLAM [58]) have been used [59]. The procedures and details of the 3D point cloud acquisition and coregistration are included in the referenced paper. However, in our study only the part of the final point cloud acquired with the mobile LiDAR is analyzed using the proposed corridor geometry evaluation procedure.

The mobile LiDAR mounted on the UGV platform during the measurements was a Velodyne VLP-16 ('Puck') LiDAR sensor (Figure 2). It is a small and compact LiDAR that is performance and power optimized for use across a variety of applications ranging from automotive, mapping, robotics, security, and smart cities, i.e., for lower speed autonomous vehicle (AV) applications. The Puck enables real-time, surround view, 3D distance, and calibrated reflectivity measurements. The main features cover a range of 100 m, up to 600,000 points/second generation, a 360° horizontal field of view and a 30° vertical field of view, and class 1 eye-safe 905 nm technology with autonomous fleet validation [60]. The distance measurement accuracy for a single point is 3 cm (1σ).

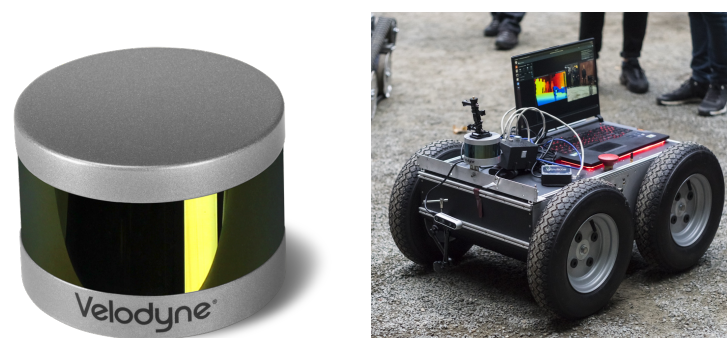


Figure 2. Velodyne VLP-16 LiDAR sensor and UGV platform.

Moreover, the scanning has also been performed with the utilization of a higher accuracy device, namely Riegl VZ-400i Terrestrial Laser Scanner (TLS) Figure 3. This survey-grade device is characterized by a 3D point position determination accuracy of 5 mm (1σ at 100 m), acquisition of up to 500,000 points/second, range from 0.5 m to 800 m, and scanning resolution of up to 0.0007° (vertical) and 0.0015° (horizontal) [61]. The scanner has a built-in Inertial Measurement Unit (IMU) used for motion estimation during changing scan positions and can be integrated with a GNSS receiver or a digital camera. Although costly and requiring the operator to carry it, the Riegl TLS can quickly obtain very dense and accurate point cloud data of a vast area.

In this paper, 3D data of the Gertruda slant (Figure 4) geometry has been processed. Renderings of the point clouds acquired with laser scanning of the Gertruda adit with the RIEGL VZ-400i TLS and a Velodyne Puck and HDL-SLAM are presented in Figure 5. Moreover, from the whole 3D point cloud representing slant geometry, an approximately 24 m long segment has been chosen (Figure 6) for analysis. Large variability of the cross sections in this part of the slant create a good test field for evaluation of the proposed diagnostic procedure. Only the point cloud acquired with SLAM has been processed using the proposed corridor geometry quality evaluation procedure to demonstrate its capabilities on a dataset obtained with an accessible, lower cost data acquisition solution. Nonetheless, a further possibility and advantages of employing it for processing highly accurate data from a survey-grade instrument are discussed in Section 6.



Figure 3. RIEGL VZ-400i Terrestrial Laser Scanner in the adit.



Figure 4. Wheeled robot during its low-speed passage through Gertruda slant.

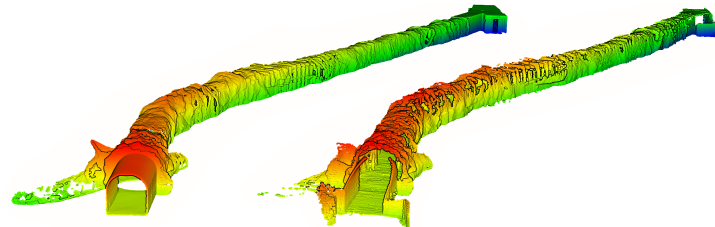


Figure 5. Renderings of a point cloud obtained with a RIEGL VZ-400i TLS (left) and a Velodyne Puck and HDL-SLAM (right). Point coloring by the Z coordinate.

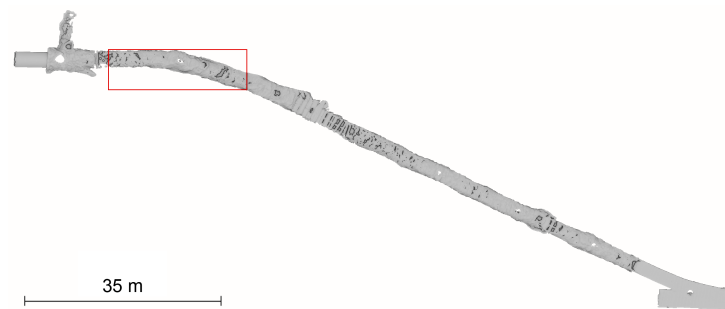


Figure 6. Top view of a 3D point cloud orthographic projection of the Gertruda slant with analyzed region marked in red.

4. Methodology

From measurement, trial one receives a spatial dataset with a massive volume of points and a specific format. As previously mentioned, raw 3D data is difficult to use for any reasoning or decision making; therefore, a method for processing is needed, which is not an easy task. If geometry evaluation is to be used in everyday practice, a simple 1D parameter is required for monitoring, but also for modeling and predicting changes in geometry.

Thus, the proposed general approach is to build a reliable 3D model from measurements, divide it into collections of cross sections, describe the 2D shape of cross sections (still multiple points) by some statistically explained features, and then again use statistical or machine learning techniques to find outliers, classes, or general patterns in tunnel geometry.

In this section, the key elements of the methodology are described. The general flow of the procedure is presented in Figure 7.

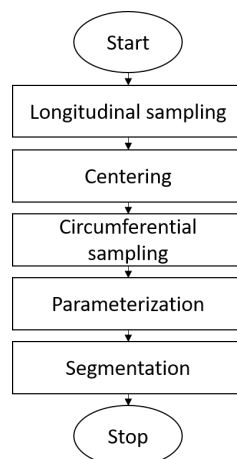


Figure 7. Flowchart of the procedure.

1. **Longitudinal sampling:** In the first step, the grid is defined in the dimension of tunnel length with a given resolution. Then, the original geometry produced by a scanner is manually sampled longitudinally according to the grid. In practice, when raw data are imported from the device to the computer, they are assembled from multiple files to a single point cloud. From this point cloud, running the bounding box filter of a given longitudinal interval (i.e., chosen cross-section separation), the slices of a point cloud are extracted. Projecting them on a plane perpendicular to the tunnel axis, the points establishing flat corridor cross sections (further called “profiles”) of the entire geometry are generated. This way, it is possible to obtain a set of cross-sectional profiles that can be further analyzed. When a set of such profiles is obtained, they are cleaned by selecting only the edge points (see Section 4.1). This way, it is possible to get rid of unnecessary points inside the corridor.

2. **Centering:** In the next step, the profiles are centered so that their shapes can be analyzed. It is a necessary preprocessing step to counteract any changes in the directions of a path of a corridor. For example, if the corridor was excavated in a perfectly straight line, centering would not be necessary because (at least in theory) the center of each profile would lie in the same position on its plane. In the horizontal direction, the median value (see Section 4.2) of each profile is subtracted (median of horizontal coordinates of points).
In the vertical direction, profiles are first normalized to the average floor level (section of a profile describing the floor is identified, and a mean value of the vertical coordinates of this section is subtracted), and then the median value is subtracted from the entire geometry in terms of vertical coordinates, so that the projection orthogonal to the length of the corridor is centered around the origin of the coordinate system.
3. **Circumferential resampling:** Centered profiles are converted to polar coordinates. This way, their shapes are “unfolded” so that the horizontal coordinate value of each point represents the angle of a point with respect to the center of a corridor, and the vertical coordinate value of each point represents the distance from the center of a corridor (such as a unit circle converted to polar coordinates becomes a constant linear function of value 1). For each profile P_i represented by a pair of vectors holding the XY coordinates of individual points, the unfolded profile Pp_i in a polar domain is represented by a pair of vectors holding the $R\Theta$ coordinates calculated as:

$$Pp_i = \begin{cases} R_i = \sqrt{(X^2 + Y^2)} \\ \Theta_i = \tan^{-1}(Y/X) \end{cases} \quad \text{for } i = 1 : N \quad (1)$$

where N is the number of profiles, the coordinate Θ denotes the angle coordinate, and the coordinate R denotes the radius coordinate (distance from the center).

Now the profile coordinates can be used as single-dimensional vectors R_i in the domain Θ , and they can be reinterpolated in the angle domain to the resolution that is common to all the profiles. First, a new domain vector Θ_r is defined with K evenly spaced points in range $(0, 2\pi)$. Then, all the vectors R_i are resampled so that $Pp_i\{R_i, \Theta_i\}$ allows to produce $Ppr_i\{Rr_i, \Theta_r\}$, where it is important to notice that the angle domain vector Θ_r is common for all Rr_i . The resampling itself is performed using a Modified Akima cubic Hermite interpolation [62]. The interpolated values are based on a piecewise function of polynomials. This way, the profiles are described by the equal amount of points evenly spaced in the domain of the angle. At this point, the evenly sampled geometry of the desired grid resolution is obtained.

4. **Parameterization:** In the beginning of parameterization, the median (see Section 4.2) profile is calculated from the entire geometry which serves as a reference model. For every profile (after circumferential resampling), their vectors Rr_i are arranged in a matrix Rr , and its median is calculated along the dimension of corridor length, which produces a new profile, also in the angle domain, such as:

$$Rr_{model} = median(Rr) \quad (2)$$

In practice, user can import additional geometry to serve as a reference model. Then, several statistics are calculated for every profile, such as:

- Total, positive, and negative deviation from the reference profile shape (see Section 4.3)—those features will be useful to describe the aspect of consistency of the excavation. Testing shows that having those 3 features together works better than using only 1 feature of total deviation, although in practice they carry the same information.
- Roughness factor (see Section 4.4)—this feature allows the user to describe the qualitative aspect of a profile in terms of how wasteful the excavation was at any given point. It is not optimal if a shape of a single profile contains a lot of variety.

- Width, height, and area of a given profile.

In total, it allows us to obtain 7 features describing the corridor along its length. Those 7 features are then used as a dataset of parameters that is used for further analysis. Those statistics can be analyzed by themselves to evaluate the geometry and draw conclusions; however, the authors propose the following method that fuses data from the statistics.

The matrix containing the statistics (Table 1) is processed using a principal component analysis (PCA) algorithm (see Section 4.5). The PCA method is known for its ability to reduce dimensionality. In practice, it means that if it is able to produce one feature that explains the vast majority of information coming from the 7-dimensional dataset, it is very practical to analyze this singular feature instead of performing 7-dimensional analysis of the data. The first component forms a diagnostic feature that describes the differences between the profiles and can be used as a working statistic for segmentation.

5. **Segmentation:** The diagnostic feature is segmented based on value thresholds. To obtain them, authors calculate a kernel density estimate of a diagnostic feature (see Section 4.6) [63] and define the thresholds as the local minima between main modes. It is performed by differential analyses of the estimated probability density function. Local minima are located at places where the first derivative is equal to 0 and the second derivative is positive. Then, profiles that belong to particular classes between those thresholds are identified. In practice, Matlab provides a function called *findpeaks* that performs this operation automatically.

Table 1. Statistics matrix.

No.	Statistics						Area
	Positive Deviation	Negative Deviation	Total Deviation	Roughness	Total Height	Total Width	
1	13.172	12.881	26.053	11.239	2.454	2.949	6.102
2	4.250	6.120	10.370	8.160	2.382	2.831	5.913
3	2.984	12.852	15.835	7.871	2.289	2.878	5.562
...
90	4.016	14.168	18.184	11.125	2.384	2.902	5.570
91	9.192	25.012	34.204	10.122	2.312	2.926	5.405
92	1.304	13.055	14.359	8.896	2.336	2.855	5.469

4.1. Boundary Detection

The detection of boundary points of a flat point cloud is performed in two steps. First, the non-convex alpha shape is generated from points, and then boundary facets are determined.

The alpha shape of a set of points is a generalization of the convex hull and a subgraph of the Delaunay triangulation [64,65]. Moreover, alpha shapes allow users to control the level of detail. Varying the parameter value from 0 to infinity can produce a set of different alpha shapes for that point set.

In the second step, boundary facets (in particular—boundary edges for 2-dimensional geometries) are identified. First, edges of an alpha shape are counted individually for each triangle. Then, edges counted only once are defined as boundary edges, which allows us to define boundary points.

4.2. Median Calculation

The median is defined as:

$$\text{median}(X) = \begin{cases} X_{(n+1)/2} & \text{for } n\%2 = 1, \\ \frac{X_{(n/2)} + X_{(n/2)+1}}{2} & \text{for } n\%2 = 0, \end{cases} \quad (3)$$

where X is a vector of values, n is the number of samples, and $\%$ denotes the operation of modulo division.

4.3. Deviation Calculation

One of the simplest statistics that can be calculated for the profiles is the deviation from the model. In order to achieve that, unfolded profiles (see step 3 in Section 4) in the angle domain are processed by subtracting from them the model profile, such as:

$$\text{dev}_i = \left| \sum_{k=1}^K Rr_i - Rr_{\text{model}} \right| \quad (4)$$

In other words, for each point on the profile (each ray from the center), the distance from the center is compared with the distance of the same point for the reference profile. Now one can take the absolute value of the result to obtain the total deviation, or just take the positive or the negative part to obtain positive (outwards) or negative (inwards) deviation.

4.4. Roughness Factor

The idea of a roughness parameter is based on the assumption that the model profile should be relatively smooth in shape and not very jagged. In order to estimate that, the derivative of the shape of each profile is analyzed, such as:

$$RF(i) = \sum_{\theta=0}^{2\pi} |\text{diff}(P(i))| \quad (5)$$

where $|\cdot|$ stands for the absolute value, $\text{diff}()$ function denotes numerical derivative, and $P(i)$ is the i th profile in a sequence. Effectively, roughness value is a sum of amplitudes of changes between consecutive points on the outline of a profile. In practice, this calculation is performed on the unfolded form of a profile, so the value of points on the profile denotes the distance from the center.

4.5. Principal Component Analysis

Principal Component Analysis is a very capable analytical tool [66]. It interprets a dataset including N samples over K variables, as a point cloud in K -dimensional feature space. The aim is to rotate and translate a local coordinate system so that the variance is maximized over new dimensions, such that the first dimension displays the greatest variance, the second dimension—second greatest variance, etc.

Such a transformed system contains new values of data, which are original data but defined over a new set of dimensions (new coordinate system). Vectors representing data over the new coordinate system are known as principal components. The new feature space describes the original dataset with the most information content located within several first principal components that carry the most information. In many cases, the information contained in several first components is sufficient due to their high information content, so PCA is regarded to be a dimensionality reduction method.

Given n observations of m -dimensional data stacked into a matrix $X \in \mathbb{R}^{n \times m}$, the principal components can be calculated using Singular Value Decomposition (SVD):

$$\frac{1}{\sqrt{n-1}}X = U\Sigma V^T, \quad (6)$$

where $U \in \mathbb{R}^{n \times n}$ and $V \in \mathbb{R}^{m \times m}$ are unitary matrices, and $\Sigma \in \mathbb{R}^{n \times m}$ contains the nonnegative real *singular values* of non-increasing magnitude ($\sigma_1 \geq \sigma_2 \geq \dots \geq \sigma_m \geq 0$). Principal components are the orthonormal column vectors of the matrix V , and the variance of the i -th component is equal to σ_i^2 .

4.6. Kernel Density Estimation

The distribution density is obtained using the kernel density estimator, which is the estimated empirical probability density function of a random variable [67,68]. For real values of the data x , the estimated distribution is given by:

$$\hat{f}_h(x) = \frac{1}{nh} \sum_{i=1}^n K\left(\frac{x-x_i}{h}\right), \quad (7)$$

where x_1, x_2, \dots, x_n are samples of unknown data, $K(\cdot)$ is the kernel smoothing function, n is the sample size, and h is the bandwidth. For this example, a Gaussian kernel is used.

The value of the bandwidth is obtained using the so-called *Silverman's rule of thumb* [68]. For the Gaussian kernel and the assumption of a Gaussian mixture, the optimal choice for h (that is, the bandwidth that minimizes the mean integrated squared error) is

$$h = \left(\frac{4\hat{\sigma}^5}{3n}\right)^{\frac{1}{5}} \approx 1.06\hat{\sigma}n^{-1/5}, \quad (8)$$

where $\hat{\sigma}$ is the estimator of a standard deviation of the samples, and n is the number of samples.

5. Results

In this section, the authors present the geometry evaluation approach on the example of a corridor section from a historical mine in Poland, shown in Figure 8. In the first place, the point cloud is segmented into slices of the same depth to acquire regular profiles. In this example, the profiles are sampled with the resolution of 25 cm; however, any different value can be chosen by the user. An example slice is shown in Figure 9a. Individual points segmented in slices are then projected onto a plane. Subsequently, Figure 9b presents an example of how those points are preprocessed in a Matlab environment. Red points are detected as boundary points, and they represent the raw form of the outlines of profiles.

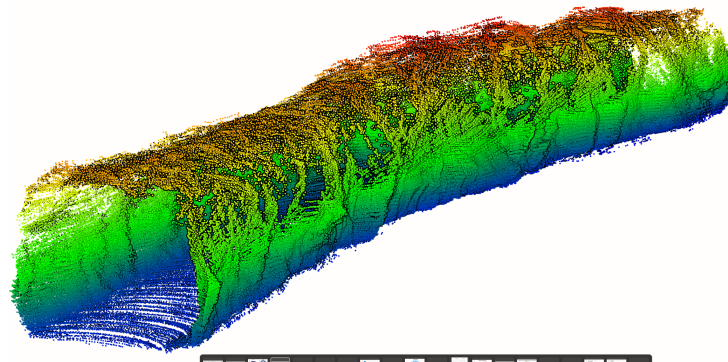


Figure 8. Point cloud of the analyzed corridor segment colored by elevation.

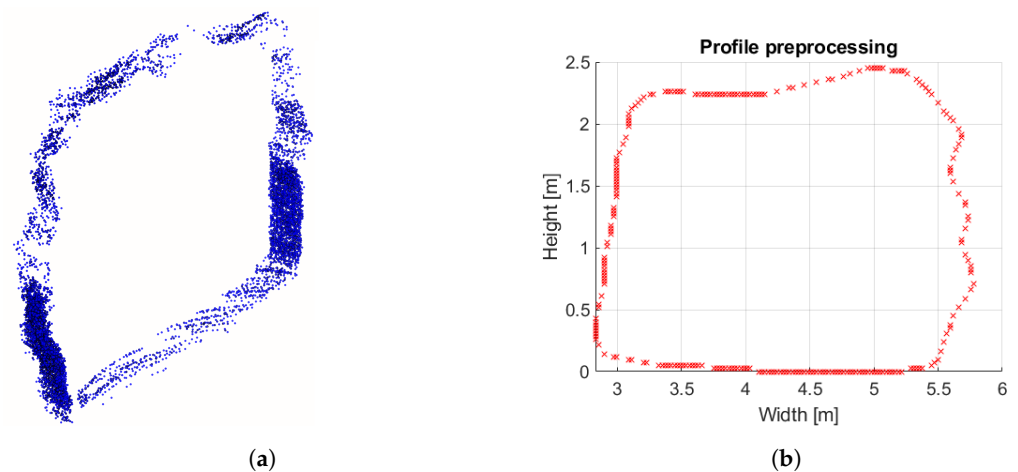


Figure 9. Identification of boundary points for further processing: (a) isometric view of an example of a point cloud slice used to generate profile; (b) preprocessing of the slices imported from the raw geometry.

In the next step, the outline is converted to polar coordinates and resampled (see Figure 10). Figure 11 presents the shapes of outlines pulled from the original point cloud provided by the 3D scan.

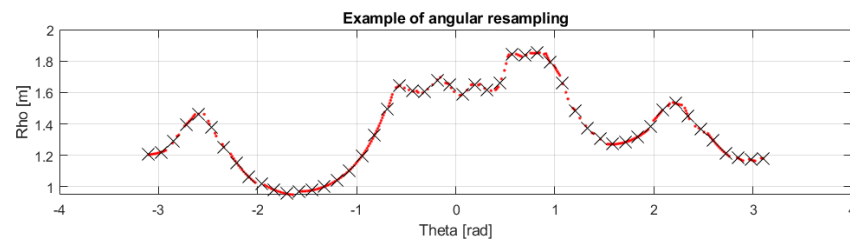


Figure 10. Example of angular resampling. Original boundary points from Figure 9b (red points) and evenly resampled data (black crosses). In this example, the amount of resampled points has been set to lower value for better visibility.

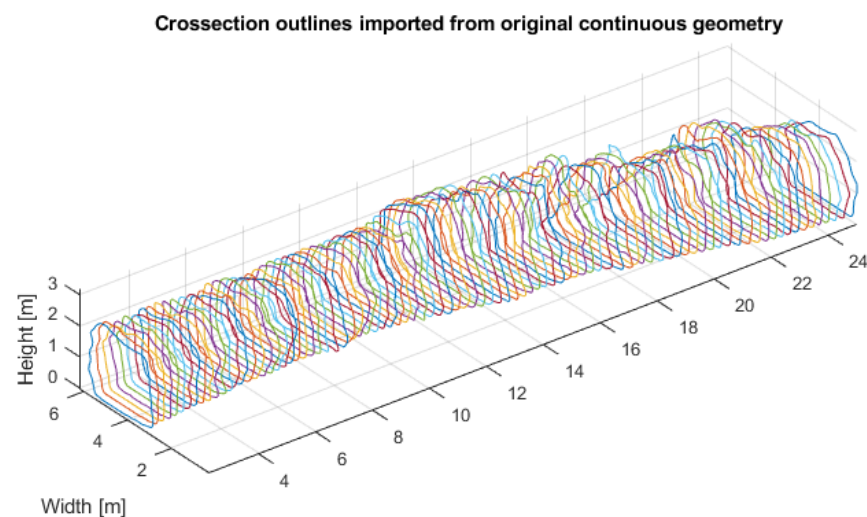


Figure 11. Overview of shapes of outlines. Dimension units are expressed in meters.

Afterwards, the profiles are centered (Figure 12) and resampled in the domain of angle (Figure 13). This way, every profile has the same amount of samples at the same angles, so they can be compared.

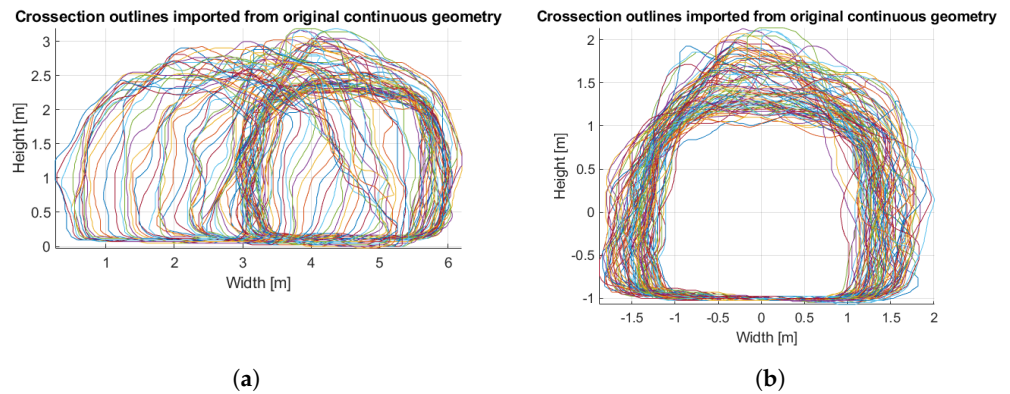


Figure 12. Comparison of profiles between and after centering: (a) orthogonal projection of profiles before centering; (b) orthogonal projection of profiles after centering.

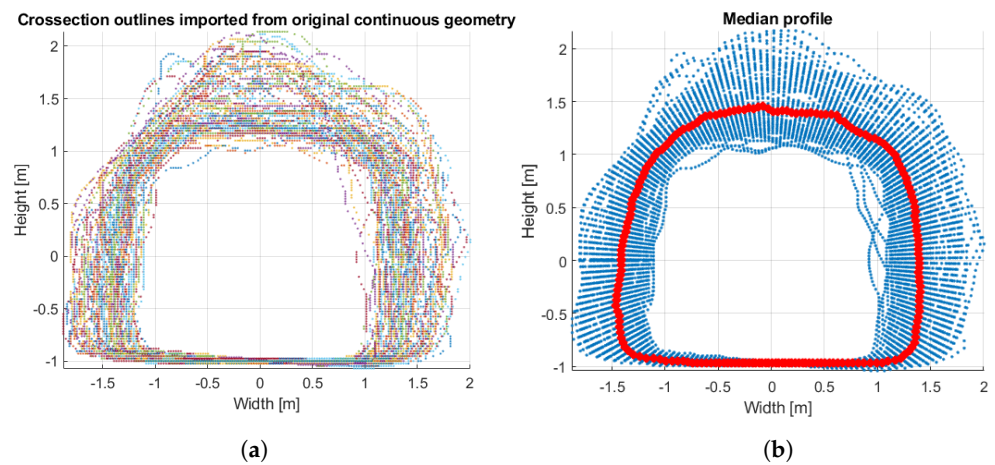


Figure 13. Comparison of point distribution of profiles before and after resampling: (a) overview of raw shapes of centered outlines before angular resampling; (b) centered outlines after angular resampling (blue) and their median (red).

When profiles are resampled, they can be parameterized with seven statistics described in Section 4 (see Figure 14).

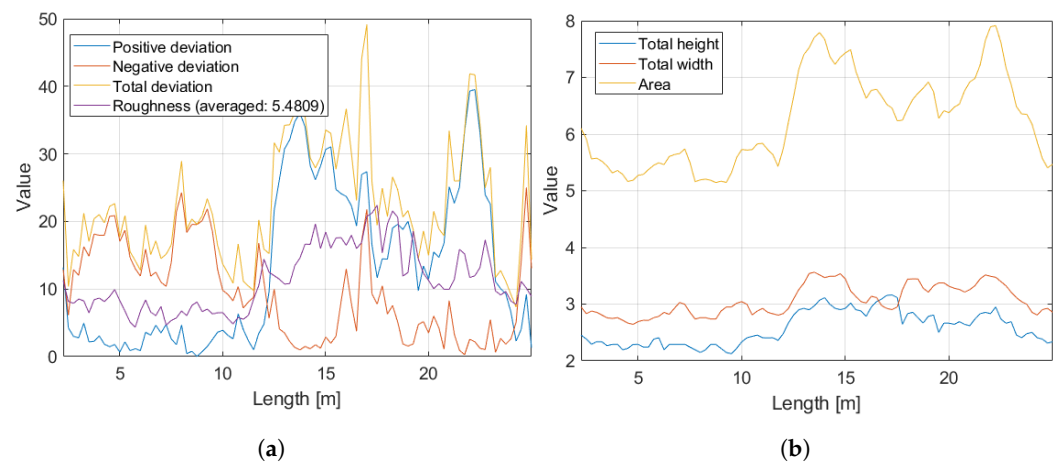


Figure 14. Statistics calculated for the resampled profiles: (a) positive deviation, negative deviation, total deviation, roughness index; (b) cross-section height, cross-section width, cross-section area.

Statistics are then passed to the PCA, and seven principal components are calculated, while the first of them is regarded as a feature useful for further segmentation based on relative variance, which for this first component was equal to 79%.

In order to achieve that, the feature is divided into segments based on its values. First, the kernel density estimate of the feature is calculated with an automatically obtained bandwidth parameter equal to 0.12 (see Section 4.6) and the normalization mode set to PDF—probability density function. It means that the integral of a function is equal to one (see Figure 15). Then, local minima of the feature are identified. Those minima define the thresholds for feature values (see Figure 16). Then, the thresholds define regimes in the domain of corridor length (see Figure 17). Median profiles of each class and original total median profile comparison together with profiles selected based on the results of segmentation has been presented in Figure 18.

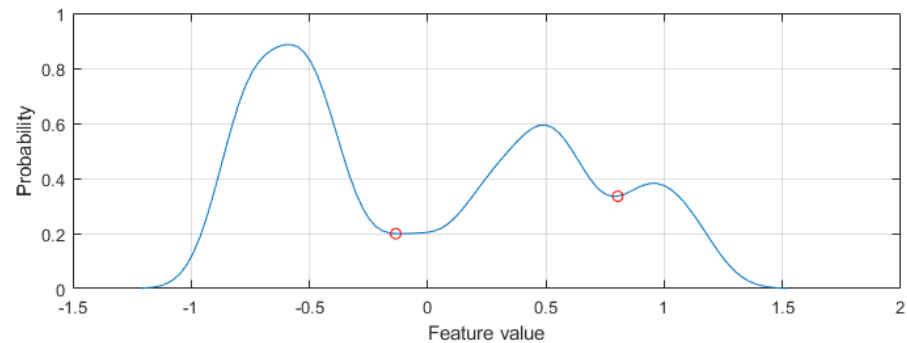


Figure 15. Kernel density estimate of feature values. Red circles indicate localized thresholds.

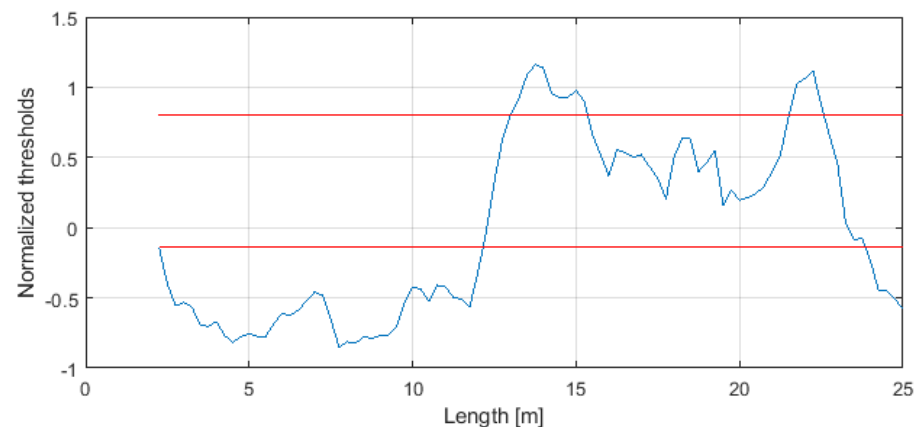


Figure 16. Obtained thresholds at values -0.13 and 0.81 for qualitative segmentation.

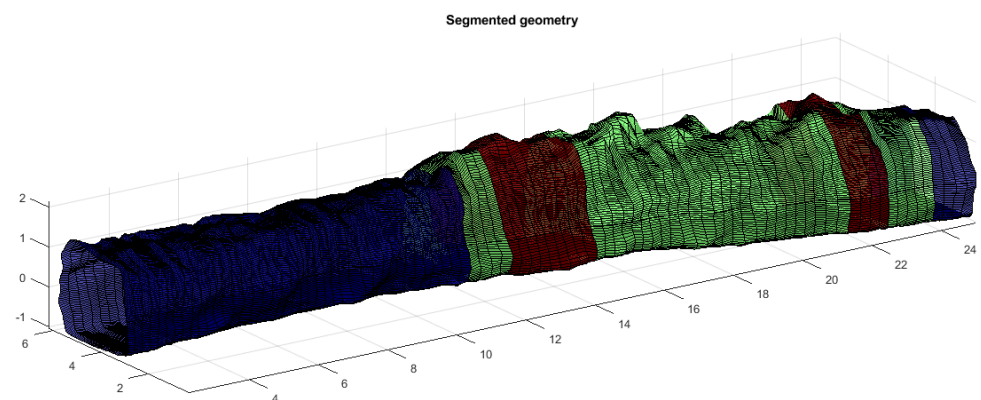


Figure 17. Segmented geometry. Colors denote assignment of individual profiles to classes. In this example, the blue class denotes the most “consistent and desirable” character of shape; green is the moderate one and red—the most irregular.

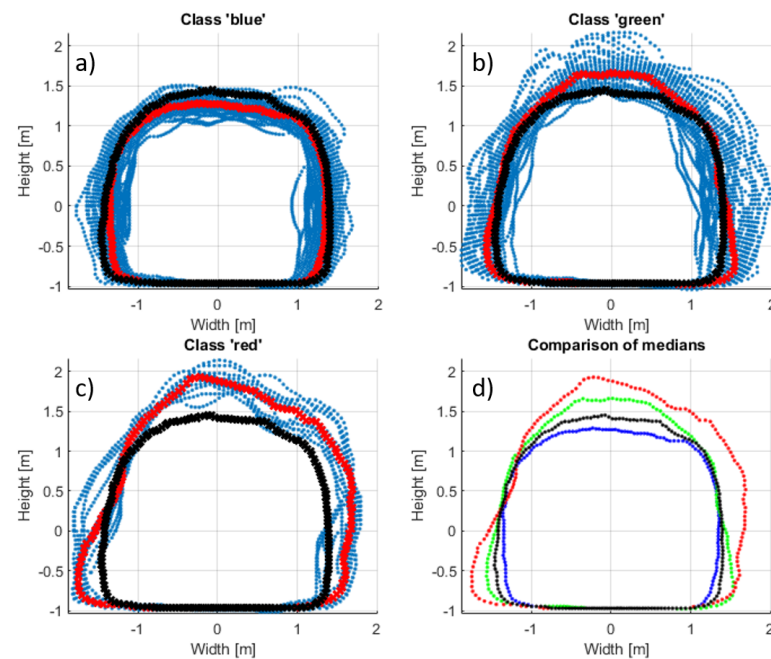


Figure 18. (Panels a–c): profiles selected based on the results of segmentation (blue points), median profile of each class (red points), and original total median profile (black points); (panel d): comparison of class medians (color-coded) with total median (black).

6. Discussion

In our study, the proposed methodology has been tested on the testbed of a closed mine corridor characterized by varied geometry due to the basic techniques employed in its creation. Such a case study could simulate a real scenario of evaluating the tunnel geometry in terms of compliance with the mining plan. In this instance, significant deviations from the plan would be in the order of tens of centimeters. As such, a point cloud obtained with a cheap SLAM solution could be used as a source of input data, despite its accuracy in the range of single centimeters. However, in cases where the desired precision of identifying deviations of the corridor geometry would be lower, e.g., during convergence monitoring, another input point cloud source of correspondingly higher measurement accuracy and resolution will be chosen. Example techniques include terrestrial laser scanning, photogrammetry (in mines with low pollution and well-lit corridors), and mobile laser scanning (for tunnels accessible by a car equipped with an MLS system).

For the proposed methodology, employing instruments of higher accuracy and resolution for measurements assures a more accurate representation of the corridor geometry mostly in the direction perpendicular to its axis. The longitudinal resolution is, however, limited by one of the initial steps of the proposed methodology—extracting slices of selected depth from the input point cloud for cross-section generation. The value of cross-section depth should be chosen individually for each use case scenario, depending on the expected or desired to be detected corridor geometry deviations regarding their dimension along the corridor. The selection of too wide cross sections may result in not detecting significant geometry disturbances or their overestimation. On the other hand, choosing too narrow point cloud slices might result in a low number of points establishing the profiles, making them an unsatisfactory representation of the real corridor geometry.

As mentioned above, geometry analysis of large underground structures consisting of dozens of kilometers of mining excavations may be of particular interest of mine maintenance services, especially geomechanical engineers or ventilation crews. The proposed methodology for spatial data utilization, combined with an appropriate statistics selection, may serve as a tool for mine ventilation optimization. As the geometry of the airways is strongly related to airflow behavior, obtained results may be strongly informative in terms of ventilation performance and indicate potential actions needed to improve the current

state. On the other hand, the results may potentially contribute to reducing the aerological hazards. Moreover, a 3D point cloud from geometry measurements adequately processed with respect to spatial mesh of underground structure development may also provide a basis for CFD methods analysis. The insights presented will constitute future work by the authors in subsequent articles based on the methodology defined in this work.

Results acquired with the introduced method at the testbed in the closed mine in Złoty Stok prove the suitability of this solution for automatic evaluation of the corridor's geometry. Moreover, it was demonstrated that for similar use cases, a point cloud obtained with SLAM manifests sufficient accuracy for subsequent processing. This shows possibilities for further automation of the proposed method utilizing an autonomous mobile robotic system. Other important directions of research include automatization of inspection of more complex scenes, (e.g., a grid of underground corridors) and testing various measurement techniques for obtaining the point cloud for different use case scenarios.

7. Conclusions

In this paper, the authors have attempted to solve the problem of geometry assessment of large underground structures. As shown in the state of the art provided, this subject is a particular matter in the field of underground mining, but also tunneling. To meet the specific requirements defined by the complex nature of this problem, several issues needed to be considered during the solution development. It covers primarily a quick and reliable measurement method allowing geometry-related spatial data acquisition with relatively low effort and capital outlay. Secondly, processing obtained data should create a field for deviation detection and variation tracking and analysis employing informative features. Such an approach in the final stage would lead to a classification of certain tunnel segments, which in terms of geometry demands taking actions aimed at maintaining mine operation according to defined specifications.

The authors proposed a simple yet effective method of assessing the quality of excavated corridors. Input data constitute the point cloud measured by a LiDAR-based scanning system. This kind of data source is not very expensive and thus may be easily accessible. During the experiment conducted by the authors, the LiDAR sensor was attached to a mobile platform. Although this solution may be beneficial from different perspectives, the process of collecting data with such a device itself can also be carried out manually. The input data type does not influence the data processing methodology. However, depending on the desired purpose, it may result in different accuracy. In practice, a digital model of underground structures may be constructed based on data captured utilizing any method, such as TLS implementation or photogrammetry.

The initial part of the proposed methodology is related to 3D data preprocessing, which is required to apply statistical parameterization and analysis. The core of the method is based on creating a multivariate parameterization of a corridor section concerning its length. The calculation of selected statistics allowed the determination of more general features. Segmentation and classification of the created segments based on those features is performed concerning the quality defined by them. The set of cross sections arranged in groups provides a global and quantitative measure of the quality of tunnel geometry.

The overriding goal for the authors of this paper was to use simple statistics to determine some informative features. Obtaining information from them particularly was not of interest; however, even by themselves, they may be useful for some specific use cases. In terms of qualitative evaluation, one could go a step further and correlate the segmentation results with one of the statistics, i.e., deviation from the reference model, or a roughness coefficient. Based on this, one could conclude that one of the classes corresponds to a better quality of excavation, while the other class to a worse one. However, this consideration is dependent on the particular use case and is not of interest within this paper.

In the long-term perspective, the progressing excavation in a given location will produce new sections of a corridor that can be assessed as a continuation of a previously

parameterized dataset. Such an approach can allow for quasi-real-time evaluation of an excavated corridor, paying attention to any deviations and eventually making corrections and maybe even adjustments to the excavation practices. Paying attention to the optimization of corridor geometry can have significant importance for the efficiency of key technological processes undertaken in underground mines.

The key advantage of the proposed approach is the ability to massively reduce the data volume at several levels of abstraction. Longitudinal and circumferential resampling allows us not only to standardize the operational structure for 3D data (which makes the analysis relatively easy and comfortable), but also to adjust the resolution to the needs of the particular case and inference, which allows making the dataset significantly smaller and the analysis significantly faster. Moreover, the parameterization step allows us to further reduce the operational dataset to only several variables in the longitudinal domain. It also makes the post-processing step (as the segmentation proposed in this paper) very efficient.

Author Contributions: Conceptualization, R.Z., J.W. and A.W.; methodology, J.W. and R.Z.; software, J.W.; validation, R.Z., J.W., A.W. and P.T.; investigation, A.W.; resources, P.T. and A.W.; data curation, P.T., A.W.; writing—original draft preparation, A.W., J.W., R.Z. and P.T.; writing—review and editing, A.W., J.W. and R.Z.; visualization, J.W.; supervision, R.Z.; funding acquisition, J.W. and A.W. All authors have read and agreed to the published version of the manuscript.

Funding: This activity has received funding from the European Institute of Innovation and Technology (EIT), a body of the European Union, under the Horizon 2020, the EU Framework Programme for Research and Innovation. This work is supported by EIT RawMaterials GmbH under Framework Partnership Agreement No. 21119 (V0T3D: Ventilation Optimizing Technology based on 3D-scanning) and No. 19018 (AMICOS. Autonomous Monitoring and Control System for Mining Plants). Scientific work published within the framework of an international project co-financed from the funds of the program of the Minister of Science and Higher Education titled “PMW” 2020-2021; contract no. 5163/KAVA/2020/2021/2.

Institutional Review Board Statement: Not applicable.

Informed Consent Statement: Not applicable.

Data Availability Statement: Not applicable.

Acknowledgments: Supported by the Foundation for Polish Science (FNP)—Jacek Wodecki.

Conflicts of Interest: The authors declare no conflict of interest.

References

1. Person, P.A.; Holmberg, R.; Lee, J. *Rock Blasting and Explosives Engineering*; CRC Press: Boca Raton, FL, USA, 1993; p. 560.
2. AFENI, T.B. Optimization of drilling and blasting operations in an open pit mine—The SOMAIR experience. *Min. Sci. Technol. (China)* **2009**, *19*, 736–739. [[CrossRef](#)]
3. Yilmaz, O.; Unlu, T. An application of the modified Holmberg–Persson approach for tunnel blasting design. *Tunn. Undergr. Space Technol.* **2014**, *43*, 113–122. [[CrossRef](#)]
4. Navarro, J.; Sanchidrián, J.; Segarra, P.; Castedo, R.; Costamagna, E.; López, L. Detection of potential overbreak zones in tunnel blasting from MWD data. *Tunn. Undergr. Space Technol.* **2018**, *82*, 504–516. [[CrossRef](#)]
5. Bieniawski, Z. Principles and methodology of design for excavations in geologic media. *Res. Eng. Des.* **1993**, *5*, 49–58. [[CrossRef](#)]
6. Brady, B.H.; Brown, E.T. *Rock Mechanics: For Underground Mining*; Springer Science & Business Media: Berlin, Germany, 1993.
7. Jang, H.; Kawamura, Y.; Shinji, U. An empirical approach of overbreak resistance factor for tunnel blasting. *Tunn. Undergr. Space Technol.* **2019**, *92*, 103060. [[CrossRef](#)]
8. Islam, M.R.; Hayashi, D.; Kamruzzaman, A. Finite element modeling of stress distributions and problems for multi-slice longwall mining in Bangladesh, with special reference to the Barapukuria coal mine. *Int. J. Coal Geol.* **2009**, *78*, 91–109. [[CrossRef](#)]
9. Di Bartolo, S.; Salvini, R. Multitemporal Terrestrial Laser Scanning for Marble Extraction Assessment in an Underground Quarry of the Apuan Alps (Italy). *Sensors* **2019**, *19*, 450. [[CrossRef](#)]
10. Benton, D.J.; Iverson, S.R.; Martin, L.A.; Johnson, J.C.; Raffaldi, M.J. Volumetric measurement of rock movement using photogrammetry. *Int. J. Min. Sci. Technol.* **2016**, *26*, 123–130. [[CrossRef](#)] [[PubMed](#)]
11. Kajzar, V.; Kukutsch, R.; Heroldova, N. Verifying the possibilities of using a 3D laser scanner in the mining underground. *Acta Geodyn. Geomater.* **2015**, *12*, 51–58. [[CrossRef](#)]

12. Kukutsch, R.; Kajzar, V.; Konicek, P.; Waclawik, P.; Ptacek, J. Possibility of convergence measurement of gates in coal mining using terrestrial 3D laser scanner. *J. Sustain. Min.* **2015**, *14*, 30–37. [[CrossRef](#)]
13. Riveiro, B.; DeJong, M.; Conde, B. Automated processing of large point clouds for structural health monitoring of masonry arch bridges. *Autom. Constr.* **2016**, *72*, 258–268. [[CrossRef](#)]
14. Teri, S.S.; Musliman, I.A. Machine learning in big lidar data: A review. *Int. Arch. Photogramm. Remote Sens. Spat. Inf. Sci.* **2019**, *42*, 641–644. [[CrossRef](#)]
15. Ibarra, J.; Maerz, N.H.; Franklin, J.A. Overbreak and underbreak in underground openings part 2: Causes and implications. *Geotech. Geol. Eng.* **1996**, *14*, 325–340. [[CrossRef](#)]
16. Mei, J.; Zhang, W.; Xu, B.; Zhu, Y.; Wang, B. Optimization Methods of Blasting Parameters of Large Cross-Section Tunnel in Horizontal Layered Rock Mass. *Geotech. Geol. Eng.* **2021**, *39*, 5309–5323. [[CrossRef](#)]
17. Singh, S.P.; Xavier, P. Causes, impact and control of overbreak in underground excavations. *Tunn. Undergr. Space Technol.* **2005**, *20*, 63–71. [[CrossRef](#)]
18. Chen, J.; Qiu, W.; Zhao, X.; Rai, P.; Ai, X.; Wang, H. Experimental and numerical investigation on overbreak control considering the influence of initial support in tunnels. *Tunn. Undergr. Space Technol.* **2021**, *115*, 104017. [[CrossRef](#)]
19. Trisugiwo, M.; Zabidi, H.; Ahmad, F. Joint analysis to evaluate geological overbreak in excavation of surge chamber cavern. *Procedia Chem.* **2016**, *19*, 751–756. [[CrossRef](#)]
20. Jang, H.; Topal, E. Optimizing overbreak prediction based on geological parameters comparing multiple regression analysis and artificial neural network. *Tunn. Undergr. Space Technol.* **2013**, *38*, 161–169. [[CrossRef](#)]
21. Liu, K.; Liu, B. Optimization of smooth blasting parameters for mountain tunnel construction with specified control indices based on a GA and ISVR coupling algorithm. *Tunn. Undergr. Space Technol.* **2017**, *70*, 363–374. [[CrossRef](#)]
22. Mohammadi, H.; Barati, B.; Chamzini, A.Y. Prediction of blast-induced overbreak based on geo-mechanical parameters, blasting factors and the area of tunnel face. *Geotech. Geol. Eng.* **2018**, *36*, 425–437. [[CrossRef](#)]
23. Foderà, G.; Voza, A.; Barovero, G.; Tinti, F.; Boldini, D. Factors influencing overbreak volumes in drill-and-blast tunnel excavation. A statistical analysis applied to the case study of the Brenner Base Tunnel–BBT. *Tunn. Undergr. Space Technol.* **2020**, *105*, 103475. [[CrossRef](#)]
24. Maerz, N.H.; Ibarra, J.; Franklin, J.A. Overbreak and underbreak in underground openings Part 1: Measurement using the light sectioning method and digital image processing. *Geotech. Geol. Eng.* **1996**, *14*, 307–323. [[CrossRef](#)]
25. Franklin, J.A.; Ibarra, J.T.; Maerz, N.H. Blast overbreak measurement by light sectioning. *Int. J. Min. Geol. Eng.* **1989**, *7*, 323–331. [[CrossRef](#)]
26. Heritage, G.; Large, A. *Laser Scanning for the Environmental Sciences*; John Wiley & Sons: Hoboken, NJ, USA, 2009.
27. Trybała, P.; Blachowski, J.; Błażej, R.; Zimroz, R. Damage Detection Based on 3D Point Cloud Data Processing from Laser Scanning of Conveyor Belt Surface. *Remote Sens.* **2021**, *13*, 55. [[CrossRef](#)]
28. Lindenbergh, R.; Uchanski, L.; Bucksch, A.; Van Gosliga, R. Structural monitoring of tunnels using terrestrial laser scanning. *Rep. Geod.* **2009**, 231–238. Available online: https://yadda.icm.edu.pl/yadda/element/bwmeta1.element.baztech-article-PWAB-0005-0007/c/httpwww_rog_gik_pw_edu_plphocadownloadnr8727.pdf (accessed on 7 December 2021).
29. Loupos, K.; Doulamis, A.D.; Stentoumis, C.; Protopapadakis, E.; Makantasis, K.; Doulamis, N.D.; Amditis, A.; Chrobocinski, P.; Victores, J.; Montero, R.; et al. Autonomous robotic system for tunnel structural inspection and assessment. *Int. J. Intell. Robot. Appl.* **2018**, *2*, 43–66. [[CrossRef](#)]
30. Amedjoe, C.G.; Agyeman, J. Assessment of effective factors in performance of an open stope using cavity monitoring system data: A case study. *J. Geol. Min. Res.* **2015**, *7*, 19–30.
31. Warneke, J.; Dwyer, J.; Orr, T. Use of a 3-D scanning laser to quantify drift geometry and overbreak due to blast damage in underground manned entries. In Proceedings of the 1st Canada-US Rock Mechanics Symposium, Vancouver, BC, Canada, 27–31 May 2007.
32. Zou, B.; Luo, Z.; Wang, J.; Hu, L. Development and Application of an Intelligent Evaluation and Control Platform for Tunnel Smooth Blasting. *Geofluids* **2021**, *2021*, 6669794. [[CrossRef](#)]
33. Che, E.; Jung, J.; Olsen, M. Object recognition, segmentation, and classification of mobile laser scanning point clouds: A state of the art review. *Sensors* **2019**, *19*, 810. [[CrossRef](#)]
34. Gikas, V. Three-dimensional laser scanning for geometry documentation and construction management of highway tunnels during excavation. *Sensors* **2012**, *12*, 11249–11270. [[CrossRef](#)]
35. Luo, Y.; Chen, J.; Xi, W.; Zhao, P.; Qiao, X.; Deng, X.; Liu, Q. Analysis of tunnel displacement accuracy with total station. *Meas. J. Int. Meas. Confed.* **2016**, *83*, 29–37. [[CrossRef](#)]
36. Chang, X.; Wang, H.; Zhang, Y.; Wang, F.; Li, Z. Bayesian prediction of tunnel convergence combining empirical model and relevance vector machine. *Meas. J. Int. Meas. Confed.* **2022**, *188*, 110621. [[CrossRef](#)]
37. Wang, D.; Luo, J.; Shen, K.; Gao, L.; Li, F.; Wang, L. Analysis of the causes of the collapse of a deep-buried large cross section of loess tunnel and evaluation of treatment measures. *Appl. Sci.* **2022**, *12*, 161. [[CrossRef](#)]
38. Tan, Z.; Li, S.; Yang, Y.; Wang, J. Large deformation characteristics and controlling measures of steeply inclined and layered soft rock of tunnels in plate suture zones. *Eng. Fail. Anal.* **2022**, *131*, 105831. [[CrossRef](#)]
39. Hou, G.Y.; Li, Z.X.; Hu, Z.Y.; Feng, D.X.; Zhou, H.; Cheng, C. Method for tunnel cross-section deformation monitoring based on distributed fiber optic sensing and neural network. *Opt. Fiber Technol.* **2021**, *67*, 102704. [[CrossRef](#)]

40. Puente, I.; González-Jorge, H.; Martínez-Sánchez, J.; Arias, P. Automatic detection of road tunnel luminaires using a mobile LiDAR system. *Meas. J. Int. Meas. Confed.* **2014**, *47*, 569–575. [CrossRef]
41. Vanneschi, C.; Mastrorocco, G.; Salvini, R. Assessment of a rock pillar failure by using change detection analysis and FEM modelling. *ISPRS Int. J. Geo-Inf.* **2021**, *10*, 774. [CrossRef]
42. Xu, T.; Xu, L.; Li, X.; Yao, J. Detection of Water Leakage in Underground Tunnels Using Corrected Intensity Data and 3D Point Cloud of Terrestrial Laser Scanning. *IEEE Access* **2018**, *6*, 32471–32480. [CrossRef]
43. Webber-Youngman, R.; Grobler, H.; Gazi, T.; Stroh, F.; van der Vyver, A. The impact of forensic laser scanning technology on incident investigations in the mining industry. *J. South. Afr. Inst. Min. Metall.* **2019**, *119*, 817–824. [CrossRef]
44. Voit, K.; Amvrazis, S.; Cordes, T.; Bergmeister, K. Drill and blast excavation forecasting using 3D laser scanning [Ausbruchprognose beim Sprengvortrieb mittels 3D-Laser scanning]. *Geomech. Tunnelbau* **2017**, *10*, 298–316.
45. Otero, R.; Lagüela, S.; Garrido, I.; Arias, P. Mobile indoor mapping technologies: A review. *Autom. Constr.* **2020**, *120*, 103399. [CrossRef]
46. Kang, Z.; Zhang, L.; Tuo, L.; Wang, B.; Chen, J. Continuous extraction of subway tunnel cross sections based on terrestrial point clouds. *Remote Sens.* **2013**, *6*, 857–879. [CrossRef]
47. Han, S.; Cho, H.; Kim, S.; Jung, J.; Heo, J. Automated and efficient method for extraction of tunnel cross sections using terrestrial laser scanned data. *J. Comput. Civ. Eng.* **2013**, *27*, 274–281. [CrossRef]
48. Yoon, J.S.; Sagong, M.; Lee, J.; Lee, K.S. Feature extraction of a concrete tunnel liner from 3D laser scanning data. *NDT E Int.* **2009**, *42*, 97–105. [CrossRef]
49. Adoko, A.C.; Jiao, Y.Y.; Wu, L.; Wang, H.; Wang, Z.H. Predicting tunnel convergence using Multivariate Adaptive Regression Spline and Artificial Neural Network. *Tunn. Undergr. Space Technol.* **2013**, *38*, 368–376. [CrossRef]
50. Fei, J.; Wu, Z.; Sun, X.; Su, D.; Bao, X. Research on tunnel engineering monitoring technology based on BPNN neural network and MARS machine learning regression algorithm. *Neural Comput. Appl.* **2021**, *33*, 239–255. [CrossRef]
51. Grilli, E.; Menna, F.; Remondino, F. A review of point clouds segmentation and classification algorithms. *Int. Arch. Photogramm. Remote Sens. Spat. Inf. Sci.* **2017**, *42*, 339. [CrossRef]
52. Remondino, F.; El-Hakim, S.; Gruen, A.; Zhang, L. Turning images into 3-D models: Developments and performance analysis of image matching for detailed surface reconstruction of heritage objects. *IEEE Signal Process. Mag.* **2008**, *25*, 55–64. [CrossRef]
53. Remondino, F.; Nocerino, E.; Toschi, I.; Menna, F. A critical review of automated photogrammetric processing of large datasets. *Int. Arch. Photogramm. Remote Sens. Spat. Inf. Sci.* **2017**, *42*, 591–599. [CrossRef]
54. Przylibski, T.A. Radon and its daughter products behaviour in the air of an underground tourist route in the former arsenic and gold mine in Złoty Stok (Sudety Mountains, SW Poland). *J. Environ. Radioact.* **2001**, *57*, 87–103. [CrossRef]
55. Muszer, A. Gold at Złoty Stok—history, exploitation, characteristic and perspectives. *Arch. Mineral. Monogr.* **2011**, *2*, 45–62.
56. Szrek, J.; Zimroz, R.; Wodecki, J.; Michalak, A.; Góralczyk, M.; Worsa-Kozak, M. Application of the infrared thermography and unmanned ground vehicle for rescue action support in underground mine—The amicos project. *Remote Sens.* **2021**, *13*, 69. [CrossRef]
57. Zimroz, P.; Trybała, P.; Wróblewski, A.; Góralczyk, M.; Szrek, J.; Wójcik, A.; Zimroz, R. Application of UAV in search and rescue actions in underground mine—A specific sound detection in noisy acoustic signal. *Energies* **2021**, *14*, 3725. [CrossRef]
58. Koide, K.; Miura, J.; Menegatti, E. A portable 3d lidar-based system for long-term and wide-area people behavior measurement. *IEEE Trans. Hum. Mach. Syst.* **2018**, *16*, 1729881419841532.
59. Trybała, P. LiDAR-based Simultaneous Localization and Mapping in an underground mine in Złoty Stok, Poland. *IOP Conf. Ser. Earth Environ. Sci.* **2021**, *942*, 012035. [CrossRef]
60. Velodyne Lidar Puck Data Sheet. Available online: <https://velodynelidar.com/products/puck/#downloads> (accessed on 7 December 2021).
61. Riegl VZ-400i Terrestrial Laser Scanner Data Sheet. Available online: http://www.riegl.com/uploads/tx_pxpriegl/downloads/RIEGL_VZ-400i_Datasheet_2020-10-06.pdf (accessed on 7 December 2021).
62. Akima, H. A new method of interpolation and smooth curve fitting based on local procedures. *J. ACM* **1970**, *17*, 589–602. [CrossRef]
63. Silverman, B.W. *Density Estimation for Statistics and Data Analysis*; Routledge: London, UK, 2018.
64. De Loera, J.; Rambau, J.; Santos, F. *Triangulations: Structures for Algorithms and Applications*; Springer Science & Business Media: Berlin, Germany, 2010; Volume 25.
65. Guibas, L.J.; Knuth, D.E.; Sharir, M. Randomized incremental construction of Delaunay and Voronoi diagrams. *Algorithmica* **1992**, *7*, 381–413. [CrossRef]
66. Moore, B. Principal component analysis in linear systems: Controllability, observability, and model reduction. *IEEE Trans. Autom. Control* **1981**, *26*, 17–32. [CrossRef]
67. Peter, D.H. Kernel estimation of a distribution function. *Commun. Stat. Theory Methods* **1985**, *14*, 605–620. [CrossRef]
68. Silverman, B.W. Density estimation for statistics and data analysis. In *Monographs on Statistics and Applied Probability*; CRC Press: Boca Raton, FL, USA, 1986; Volume 26.